AGU PUBLICATIONS

JGR

Journal of Geophysical Research: Atmospheres

RESEARCH ARTICLE
10.1002/2015JD023863

Key Points:
- Measurements of turbulent exchange are presented and analyzed for a lake on the Tibetan Plateau
- The wave pattern in shallow lakes gives a larger roughness length for momentum
- Free convection gives a square root dependence of latent heat flux on wind speed

Correspondence to:
B. Wang,
wangbinbin@itpcas.ac.cn

Citation:
Wang, B., Y. Ma, X. Chen, W. Ma, Z. Su, and M. Menenti (2015), Observation and simulation of lake-air heat and water transfer processes in a high-altitude shallow lake on the Tibetan Plateau, *J. Geophys. Res. Atmos.*, *120*, 12,327–12,344, doi:10.1002/2015JD023863.

Received 28 JUN 2015
Accepted 10 NOV 2015
Accepted article online 13 NOV 2015
Published online 16 DEC 2015

Observation and simulation of lake-air heat and water transfer processes in a high-altitude shallow lake on the Tibetan Plateau

Binbin Wang[1,2,3,4], Yaoming Ma[1,2,3], Xuelong Chen[4], Weiqiang Ma[1,2], Zhongbo Su[4], and Massimo Menenti[5]

[1]Key Laboratory of Tibetan Environment Changes and Land Surface Processes, Institute of Tibetan Plateau Research, Chinese Academy of Sciences, Beijing, China, [2]CAS Center for Excellence in Tibetan Plateau Earth Sciences, Chinese Academy of Sciences, Beijing, China, [3]University of Chinese Academy of Sciences, Beijing, China, [4]Faculty of Geo-Information Science and Earth Observation, University of Twente, Enschede, Netherlands, [5]Faculty of Civil Engineering and Earth Sciences, Delft University of Technology, Delft, Netherlands

Abstract Lakes are an important part of the landscape on the Tibetan Plateau. Most of the Plateau lakes' area has been expanding in recent years, but lake-atmosphere energy and water interaction is poorly understood because of a lack of observational data and adequate modeling systems. Based on the eddy covariance observation over a high-altitude shallow and small lake (the small Nam Co Lake) during an ice-free period from 10 April to 30 August 2012, this study analyzes the lake-air heat and water vapor turbulent transfer processes and evaluates two popular lake-air exchange models: a bulk aerodynamic transfer model (B model) and a multilayer model (M model). Our main results are as follows: (1) observations show that the bulk transfer coefficient (C_E) and roughness length (z_{oq}) for water are higher than those for heat (C_H and z_{0h}), especially under low wind speed; (2) both models underestimate turbulent fluxes due to inaccurate values of the Charnock coefficient (α) and the roughness Reynolds number (R_r) which are both important parameters for calculating the roughness length for momentum (z_{0m}) over water; (3) α within a reasonable range of 0.013–0.035 for rough flow and R_r for smooth flow ($R_r = 0.11$) are 0.031 and 0.54, respectively, by our observation. The wave pattern of shorter wavelength gives a larger z_{0m} in the small and shallow lake; and (4) the B model and the M model gave consistent results, and both models are more suitable for simulation of turbulent flux exchange after z_{0m} optimization.

1. Introduction

The Tibetan Plateau (TP) with an average altitude of more than 4000 m above sea level (asl) is referred to as "Asia's water tower" and the "Third Pole of the Earth" [*Qiu*, 2008]. With an estimated 32,843 total lakes, approximately 1204 of which are larger than 1 km^2 and the rest of which are smaller than 1 km^2, lakes play an important role in the water cycle and energy budget of the "Third Pole" area [*Wang and Dou*, 1998; *Zhang et al.*, 2014]. Recent studies have shown that the number of lakes on the TP is increasing, and most of the lakes have been expanding because of the effects of warming climate through increased precipitation and glacier melt [*Liu et al.*, 2010; *Wang et al.*, 2013; *Yang et al.*, 2014; *Zhang et al.*, 2011]. Vertical turbulent heat fluxes (latent heat flux (LE) and sensible heat flux (H)) over the lake-air interface are fundamental driving forces for the atmospheric boundary layer growth of lakes, and these are vital variables for characterizing the lake-air interaction in numerical climate models [*Daniel*, 1998; *Haginoya et al.*, 2009; *Jin et al.*, 2010; *Xiao et al.*, 2013]. However, due to harsh climatic conditions and the difficulties associated with measuring these parameters over the water surface, little attention was paid to lake-air interactions during previous TP energy and water cycle experiments (such as the GAME/Tibet-Global Energy and Water Cycle Experiment, and the CAMP/Tibet-Coordinated Enhanced Observing Period Asia-Australia Monsoon Project) [*Ma et al.*, 2008, 2002, 2006; *Tanaka et al.*, 2001, 2003; *Yang et al.*, 2008].

Observations in low-land lakes have shown that heat and water exchange between lakes and the overlying atmosphere differs from the exchange between land and atmosphere; additionally, lakes can influence local climate via heat and water vapor transport processes through lake-land breeze circulation and the alteration of local precipitation [*Blanken et al.*, 2003, 2011; *Lee et al.*, 2014; *Liu et al.,* 2009; *Venalainen et al.*, 1999; *Verburg and Antenucci*, 2010; *Xiao et al.*, 2013]. The lake-air heat and water exchange is not only related to the lake surface conditions, such as lake surface temperature, ice coverage, lake depth, and waves, but is also influenced by

the surrounding environment and atmospheric conditions [*Blanken et al.*, 2003; *Blanken et al.*, 2011; *Gao et al.*, 2006; *Panin et al.*, 2006; *Spence et al.*, 2011]. For example, A stable/unstable atmosphere can reduce/increase the heat loss from lake water [*Brutsaert*, 1982]. Due to the relatively greater heating and cooling effect from the surrounding land, small lakes generally have a more variable atmospheric boundary layer than big lakes [*Deng et al.*, 2012; *Katsaros*, 1998]. There has been very limited research on heat and water vapor processes in the large lakes on the TP and little on small and shallow lakes. A few studies have used eddy covariance (EC) observations to examine the high-altitude lakes of the TP. For example, *Biermann et al.* [2013] analyzed differences in water and heat flux transport over water and grassland by combining footprint analysis with short-term EC observations on the shoreline of the small Nam Co Lake (4715 m asl); *Liu et al.* [2014] analyzed the heat and water exchange coefficients (i.e., roughness lengths and bulk transfer coefficients) over Lake Erhai (1978 m asl) on the southeast edge of the TP; and *Li et al.* [2015] reported a persistently unstable atmosphere over the Lake Ngoring (4274 m asl) on the eastern plateau. However, few studies have simulated the turbulent flux transport of heat and water between high-altitude lakes and the atmosphere [*Biermann et al.*, 2013].

To better understand heat and water vapor exchange and to find the appropriate modeling approach for the small and shallow lakes on the TP, this study employs two popular lake-air heat and water exchange models of different complexity, the widely used Bulk aerodynamic transfer model [*Fairall et al.*, 1996b; *Verburg and Antenucci*, 2010] and the experiment-based multilayer model [*Foken*, 1979, 1984], hereafter referred to as the B model and M model, respectively. The two models have different structures and methods of representing turbulent diffusion over the water surface of a lake. In the B model, *H*, LE, and wind stress are related to traditional meteorological observations (such as wind speed, water temperature, air temperature, and air humidity) through bulk transfer coefficients which can be parameterized using the roughness lengths for momentum, heat, and water vapor [*Beljaars and Holtslag*, 1991; *Brutsaert*, 1999; *Fairall et al.*, 1996b; *Katsaros*, 1998; *Liu et al.*, 1979; *Pond et al.*, 1974; *Rouse et al.*, 2003; *Smith*, 1988; *Verburg and Antenucci*, 2010]. In principle the M model describes much better heat and vapor transfer, since it takes into account contributions from different planetary boundary layer (PBL) sublayers: the molecular layer, buffer layer, and turbulent layer [*Foken*, 1984]. For each layer, various atmospheric stratification exchange coefficients and experimental constants are used [*Foken,* 1979, 1984; *Foken and Skeib*, 1983; *Mangarella et al.*, 1973; *Merlivat and Coantic*, 1975; *Panin et al.*, 2006].

The roughness length for momentum is a basic and fundamental parameter in lake-air heat flux modeling. It is highly variable with different water surface conditions, and scientists have attempted to quantify it by taking into account field information on wave height, wavelength, and wave age [*Ataktürk and Katsaros*, 1999; *Charnock*, 1955; *Donelan et al.*, 1993; *Fairall*, 1996; *Gao et al.*, 2006; *Smith et al.*, 1992]. At similar wind and fetch conditions, waves generated in shallow water have a smaller wave height and a shorter wavelength than in deep water [*Whalin et al.*, 1984]. The effective roughness length for momentum increases with wave height and decreases with wavelength [*Menenti and Ritchie*, 1994; *Taylor et al.*, 1989]. It has been reported that roughness length for momentum is higher for coastal water than open sea water [*Gao et al.*, 2009]. *Panin and Foken* [2005] described a correction on heat flux transfer to take into account the dependence of wave height on water depth [see also *Panin et al.*, 2006]. Another feature relevant to the thermal stratification of lake water is salinity, which is 1198 mg L^{-1} in the large Nam Co Lake [*Wang et al.*, 2009]. Assuming the salinity in the small Nam Co Lake is similar or higher, a water density gradient may be established like in a solar pond [*Hull*, 1979], which reduces mixing in the water and increases the surface water temperature. Because of the higher temperature in the surface water layer, higher air specific humidity close to the water surface is likely to occur. Due to higher air temperature and humidity at the water-air interface, free convective conditions (FCCs) [*Zhou et al.*, 2011], i.e., when buoyancy is dominant over shear, are likely to occur. In this study, we use the term FCCs to refer to the occurrence of free convection in the surface layer.

To achieve the goals of understanding the characteristics of lake-air interaction, testing the applicability of the models, and improving their parameterization scheme over high-altitude shallow lakes, a long-term eddy covariance observation system was installed in the shallow small Nam Co Lake in April 2012. The eddy covariance observations are used as direct measurements and validation data in this paper. After describing the study site and methods in sections 2 and 3, respectively, results and discussion are presented in section 4, followed by conclusions in section 5. Specifically, observations from 10 April through 30 August 2012 are analyzed in section 4.1, providing a general background for the simulations. Next, we compare the models, showing that they perform similarly, and choose the B model for parameter sensitivity analysis in section 4.2. In section 4.3,

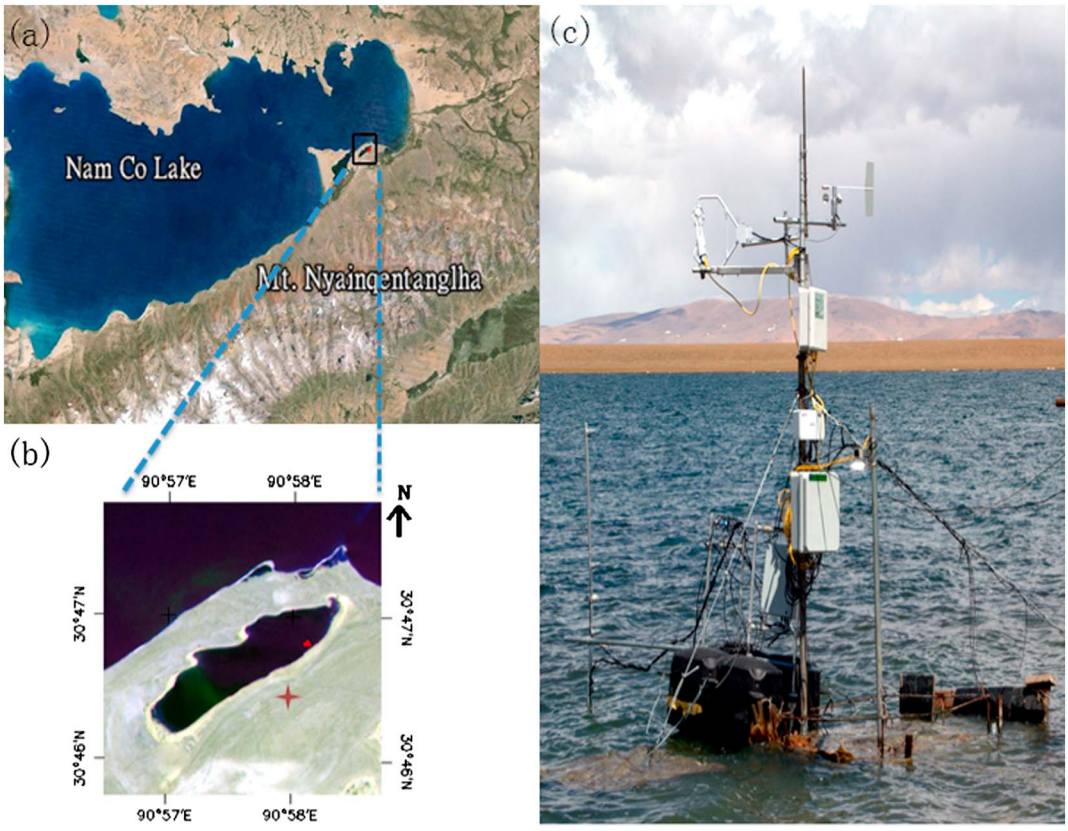

Figure 1. (a) Map of the Nam Co Lake area; (b) map of the study area; the red triangle and the red cross are the positions of the EC observation system and the Nam Co station, respectively; the horizontal scale is about 3.5 km × 3.5 km. (c) Photo of the EC observation system.

we discuss the bias in the roughness length for momentum and heat flux between the simulations and observations; in section 4.4, we demonstrate that inaccurate parameters for roughness length for momentum result in underestimation of the simulated heat flux. Finally, the limitations of the models, especially under FCCs, are documented in section 4.5.

2. Site Description

The small Nam Co Lake (30°46′55″N, 90°58′10″E) is a very shallow lake located at an altitude of approximately 4715 m asl and situated between Nam Co Lake (the second largest lake on the TP, approximately 1980 km^2) and the Nyainqentanglha Mountains (glacier-capped mountains with an altitude ranging from approximately 5300 m to 6400 m asl) on the TP (Figure 1a). There is a relatively flat area between the Nam Co Lake and the mountains. The dominant land cover is a homogeneous ecotone composed of alpine meadows and steppe grasses, with mixed vegetation including *Kobresia macrantha* and *Stipa purpurea* [*Miehe et al.*, 2011; *Wei et al.*, 2012]. The land-lake breeze circulation in the area of Nam Co Lake and the Nyainqentanglha Mountains displays obvious diurnal variations [*Biermann et al.*, 2013; *Gerken et al.*, 2014; *Zhou et al.*, 2011]**.** The wind mostly blows from the lake area during the day and from the land at night. The study area lies in the transition region between the semihumid zone and the semiarid zone; it is influenced by the westerly wind and the southwest monsoon system. The annual mean air temperature is approximately 0°C, and the annual mean wind speed is approximately 4.04 m s^{-1} based on PBL tower measurements on land taken from 2007 to 2012 in the Nam Co Monitoring and Research Station for the Alpine Environment (Nam Co station) [*Ma et al.*, 2009]. Precipitation mainly occurs during the monsoon period (May to October), and the multiyear average (from 2007 to 2011) is approximately 505 mm [*Zhou et al.*, 2013].

The small Nam Co Lake stretches from northeast to southwest and measures approximately 2620 m by 510 m in size with a generally rectangular shape and an area of approximately 1 km^2. The lake eddy covariance (EC)

observation system is situated 8 m offshore (red triangle in Figure 1b) and approximately 500 m from the northern shore. The water depth around the lake EC system is approximately 1.5 m. The PBL tower at the Nam Co station (red cross in Figure 1b) is approximately 1 km away from the lake EC system.

The lake EC system (Figure 1c) includes a sonic anemometer (CSAT3, Campbell Scientific, Inc.) and an open path CO_2/H_2O analyzer (LI-7500A, LI-COR Biosciences), which are installed approximately 2.7 m above the water surface. The CSAT3 faces west and the LI-7500A is situated 25 cm south of the CSAT3. Wind velocity, temperature, and humidity are recorded by a data logger (CR5000, Campbell Scientific, Inc) at a frequency of 10 Hz. Upward and downward short-wave and long-wave radiation (CNR4, Kipp & Zonen) are measured at a fixed height of 1.5 m above the water surface. Three fixed lake water temperature sensors were installed (Pt100, at 5 cm, 10 cm, and 20 cm), avoiding direct exposure to sunlight. In addition, five fixed water temperature sensors were also placed at 5 cm, 9 cm, 15 cm, 31 cm, and 65 cm depth. All the instruments are fixed onto concrete platforms in the water.

3. Methods

3.1. Description of the Two Models

3.1.1. Bulk Aerodynamic Transfer Model

The modeled values for H and LE are linearly proportional to the stability-dependent bulk transfer coefficients, and they are also affected by wind velocity and the gradients of temperature and humidity between water and atmosphere, respectively [*Verburg and Antenucci*, 2010; *Vickers and Mahrt*, 2010; *Vincent et al.*, 2008]. H and LE then can be expressed as follows:

$$H = \rho_a c_p C_H U_z (T_0 - T) \tag{1}$$

$$\mathrm{LE} = \rho_a L_v C_E U_z (q_0 - q) \tag{2}$$

where ρ_a is the air density (kg m^{-3}); c_p is the specific heat of air (1005 J kg^{-1} K^{-1}); L_v is the latent heat of vaporization (J kg^{-1}); U_z (m s^{-1}) is the wind speed at the reference height (2.7 m); T (K) and q (kg kg^{-1}) are the temperature and specific humidity at the reference height, and T_0 (K) and q_0 (kg kg^{-1}) are the same quantities at the water surface; C_H and C_E are the bulk transfer coefficients for heat and water, respectively. In oceanic research, the roughness lengths for heat and water (z_{0h} and z_{oq}) are assumed to be the same [*Zeng et al.*, 1998]. Thus, the B model used in this study assumes that C_H and C_E are equal and given by the following equation:

$$C_H = C_E = k^2 \Big/ \left\{ \left[\ln\left(\frac{Z_m}{z_{0m}}\right) - \psi_M \right] \left[\ln\left(\frac{Z_m}{z_{0h}}\right) - \psi_H \right] \right\} \tag{3}$$

where $k = 0.4$ is the von Kármán constant; Z_m (m) is the observational height; and ψ_M and ψ_H are atmospheric stability correction functions for momentum and heat/water vapor, respectively, with different forms in stable [*Dyer*, 1967] and unstable [*Businger et al.*, 1971] atmospheric conditions. These functions are related to the stability parameter (Z_m/L), where L is the Monin-Obukhov length given by equation (4). The roughness length for momentum (z_{0m}) is expressed as a combination of smooth flow ($\alpha \frac{u_*^2}{g}$) and rough flow ($R_r \frac{v}{u_*}$) [*Fairall et al.*, 1996b; *Verburg and Antenucci*, 2010] by equation (5); and z_{0h} is related to the roughness Reynolds number (Re) and was defined as equation (6) by *Zeng et al.* [1998].

$$L = \frac{-\rho_a u_*^3 T_v}{kg\left(\frac{H}{c_p} + 0.61 \frac{T \times \mathrm{LE}}{L_v}\right)} \tag{4}$$

$$z_{0m} = \alpha \frac{u_*^2}{g} + R_r \frac{v}{u_*} \tag{5}$$

$$z_{0h} = z_{0m} \exp\left(-2.67 \ Re^{1/4} + 2.57\right) \tag{6}$$

where T_v is the virtual air temperature (K); g is the gravitational acceleration (m s^{-2}); α is the Charnock number (0.013 in sea-atmosphere research), which depends on wave-field conditions and the observational environment; the roughness Reynolds number for smooth flow ($R_r = 0.11$) is related to the viscous shear in sea dynamic roughness length parameterizations [*Fairall et al.*, 1996b]; v is the kinematic viscosity of air ($m^2\ s^{-1}$) [*Massman*, 1999]; u_* is the friction velocity; and Re can be expressed as follows: $Re = u_* z_{0m}/v$.

3.1.2. Multilayer Model

The transformed universal energy exchange formula for near-surface layers of the atmosphere [*Foken*, 1984] can be expressed as follows:

$$X(z) - X(0) = \overline{X'w'} \int_0^z \frac{f\left(\frac{z}{L}\right)\mathrm{d}z}{v_t + v_m} \tag{7}$$

where X denotes the wind velocity for momentum, the temperature for heat, or the specific humidity for water vapor with the observational heights defined by "z" and "0" in the parentheses; w' is the fluctuation in the vertical wind component; v_t is the turbulent exchange coefficient, which can be expressed as $v_t = kvu_*$ [*Foken*, 1984; *Monin and Yaglom*, 1965]; and v_m is the molecular exchange coefficient, referred to as the kinematic viscosity of air. The inverse of the integral term in equation (7) is the so-called profile coefficient Γ [*Foken*, 1979, 1984; *Panin et al.*, 2006], and it can be expressed in four-layer integration as follows:

$$\Gamma = \left(\underbrace{\int_0^{\delta} \frac{\mathrm{d}z}{v_m}}_{(1)} + \underbrace{\int_{\delta}^{\delta_z} \frac{\mathrm{d}z}{v_m + v_t}}_{(2)} + \underbrace{\int_{\delta_z}^{\delta_D} \frac{\mathrm{d}z}{v_t}}_{(3)} + \underbrace{\int_{\delta_D}^{Z_m} \frac{\phi\left(\frac{z}{L}\right)\mathrm{d}z}{v_t}}_{(4)} \right)^{-1} \tag{8}$$

The profile coefficient divides the atmosphere into four layers: a molecular boundary layer (1), a buffer layer (2), a turbulent layer without stability correction (3), and a turbulent layer (4) with the stability corrective function $\phi(z/L)$. This profile coefficient is related only to the thicknesses of the molecular boundary layer (δ), the buffer layer (δ_z), and the dynamical sublayer (δ_D), as well as Z_m, u_*, and L. More details about δ, δ_z, and δ_D can be found in *Foken* [1984]. Finally, the integral formulas for unstable, neutral, and stable atmospheres can be given, respectively, as follows:

$$\Gamma = \frac{ku_*}{\left[\frac{v_m}{v_{Xm}} a \times k + 4k + \ln\frac{\zeta_c L u_*}{20v} + \frac{1}{n}\left(1 - \frac{Z_m}{L \times \zeta_{c1}}\right)^{-n}\right]} \quad \zeta \le -0.075 \tag{9}$$

$$\Gamma = \frac{ku_*}{\left[\frac{v_m}{v_{Xm}} a \times k + 4k + \ln\frac{\zeta_c L u_*}{20v} + \ln\frac{Z_m}{\zeta_c L}\right]} \quad -0.075 \le \zeta \le 0.16 \tag{10}$$

$$\Gamma = \frac{ku_*}{\left[\frac{v_m}{v_{Xm}} a \times k + 4k + \ln\frac{\zeta_c L u_*}{20v} + \frac{1}{m}\left(1 - \frac{Z_m}{L \times \zeta_{c2}}\right)^{-m}\right]} \quad \zeta \ge 0.16 \tag{11}$$

where $\frac{v_m}{v_{Xm}} = Pr$ (the Prandtl number), $\zeta_c = \frac{\delta_D}{L}$, $a = 6$, $n = 0.5$, $m = -2$, $\zeta_{c1} = -0.075$, and $\zeta_{c2} = 0.16$. As the simulated heat flux is usually underestimated in the M model for small lakes [*Panin et al.*, 2006], we selected the smallest δ_D by setting $\zeta_c = \zeta_{c1}$ for unstable conditions, $\zeta_c = \zeta_{c2}$ for stable conditions, and $\zeta_c L = \max(|\zeta_{c1} L|, |\zeta_{c2} L|)$ for neutral conditions. After derivation of the profile coefficient Γ, H and LE can be obtained using equations (12) and (13):

$$H = \rho_a c_p \Gamma (T_0 - T) \tag{12}$$

$$\mathrm{LE} = \rho_a L_v \Gamma (q_0 - q) \tag{13}$$

3.2. Data Preparation for the Models

3.2.1. EC Data Processing

The EC method for high-frequency sample data was chosen to determine heat, water vapor, and momentum flux. The "Turbulence Knight 3" (TK3) software package developed by Bayreuth University was used to process the turbulence data [*Mauder and Foken*, 2015] (https://zenodo.org/record/20349#). The processing included time lag compensation, spike removal, planar fit coordinate rotation [*Wilczak et al.*, 2000], spectral correction [*Foken et al.*, 2004], conversion of buoyancy into sensible heat, and correction for density fluctuations (Webb correction) to determine the flux of scalar quantities such as H_2O [*Foken et al.*, 2004; *Webb et al.*, 1980]. Values of H, LE, and friction velocity were produced at half-hourly intervals, together with data quality indicators 1–9 (1 indicates high quality, 9 low quality) [*Foken et al.*, 2004]. Footprint analysis [*Göckede et al.*, 2004] was used to identify observations collected when the small Nam Co Lake was the dominant source area. *Biermann et al.* [2013] showed that the observed turbulent heat flux for conditions with wind direction from the lake can represent the land surface type of "water surface." We selected the turbulent flux data from specific wind sectors (wind direction >240° and wind direction <40°, with north at 0° and the azimuth increasing clockwise) and used the water surface measurements from the footprint analysis. After passing through the footprint requirements and data quality standards (quality indicators < 4), there are 2268 half-hourly data points that were used for simulation and validation.

3.2.2. Implementation of Model Simulation

Because of the water level variations in the lake surface, it is difficult to determine lake surface skin temperature (T_0). It is well known that the lake surface skin temperature is different from the surface mixed (water) layer temperature because of the cool-skin and warm-layer effects [*Fairall et al.*, 1996a]. However, because of the strong wind-driven mixing in the lake's surface water and the very high correlation coefficients that have been found in various water temperature observations (at 5 cm, 10 cm, and 20 cm), we assume that using the mixed layer temperature (at 5 cm depth) as T_0 will not introduce significant uncertainty in our study. Next, the surface specific humidity (q_0) can be obtained from the saturated vapor pressure (e_{sat}, units: Pa) at T_0 and $q_0 = 0.622e_{sat}/p$, where p is the air pressure (Pa). Finally, T, q, U_z, p, L, u_*, H, and LE can all be obtained by processing the EC measurements. In particular, T and q from the EC observations (at a height of 2.7 m) were validated using the PBL tower profile observations (at a height of 2 m) at the Nam Co station, showing very consistent magnitudes and variations.

Thus, the input data for the model simulation are T_0, T, U_z, q, and p. The parameters ρ_a, L_v, T_v, and v can all be obtained from the input data. In the B model, z_{0h} and $C_H \& C_E$ can be determined from equations (6) and (3), respectively, and the stability-corrected values for H, LE, and u_* can be iteratively obtained from equations (1)–(6). In the M model, values for L and u_* can be obtained from the input data and the initial z_{0m}. The profile coefficient Γ can be calculated using equations ((9)–(11)), and values for H and LE can be obtained using equations (12) and (13).

3.2.3. Obtaining FCCs and Roughness Lengths

FCCs, which can be triggered by the appearance of clouds and changes in wind direction during the diurnal thermally forced land-lake breeze circulation, occurred over nearly 40% of the observational period at the Nam Co station [*Zhou et al.*, 2011]. These FCCs correspond to high buoyancy flux, strongly reduced wind speed, and an extremely unstable atmosphere. These characteristics of FCCs lead to higher values of the bulk transfer coefficients in equations (1) and (2). For the half-hourly data in our research, we used both $Z_m/L < -0.3$ and $U_z < 3\ \mathrm{m\ s^{-1}}$ to represent conditions influenced by the FCCs.

The roughness lengths are important parameters for parameterization of bulk transfer coefficients in heat flux modeling of the water surface. These values can be obtained through large amounts of observational data under both neutral and nonneutral atmospheric conditions, and the optimal values of roughness lengths should correspond to the peak of its frequency distribution [*Yang et al.*, 2002, 2008]. Although this method does not give an exact value for the water surface subject to wave fields and variable lake environments, it can be used to calculate z_{0m}, z_{0h}, and z_{0q} by predicting their possible ranges of variation. The equations are as follows [*Foken*, 2008]:

$$\ln(z_{0m}) = \ln(Z_m) - \psi_M\left(\frac{z_{0m}}{L}, \frac{Z_m}{L}\right) - \frac{kU_z}{u_*} \tag{14}$$

$$\ln(z_{0h}) = \ln(Z_m) - \psi_E\left(\frac{z_{0h}}{L}, \frac{Z_m}{L}\right) - \frac{k(T_0 - T)}{T_*} \tag{15}$$

$$\ln(z_{0q}) = \ln(Z_m) - \psi_E\left(\frac{z_{0q}}{L}, \frac{Z_m}{L}\right) - \frac{k(q_0 - q)}{Q_*} \tag{16}$$

where u_*, T_*, and Q_* are the related Monin-Obukhov similarity scaling parameters [*Fairall et al.*, 1996b; *Panofsky and Dutton*, 1984], which can be derived from observational data in the equations $T_* = {}^{-}H/\rho_a C_p u_*$ and $Q_* = {}^{-}\mathrm{LE}/\rho_a L_v u_*$, respectively. The observed roughness lengths for momentum, heat, and water vapor that are used to evaluate the models can be obtained from equations (14)–(16).

3.3. Error Metrics

To quantitatively analyze the difference between model simulations and observations, we used the correlation coefficient (R), the mean absolute error (MAE), and the root-mean-square error (RMSE), which are defined as follows:

$$\mathrm{MAE} = \frac{\sum_{i=1}^{n} |S_i - O_i|}{n} \tag{17}$$

$$\mathrm{RMSE} = \sqrt{\frac{\sum_{i=1}^{n} (S_i - O_i)^2}{n}} \tag{18}$$

where n is the total number of observations, S_i is the simulated results, and O_i is the observations.

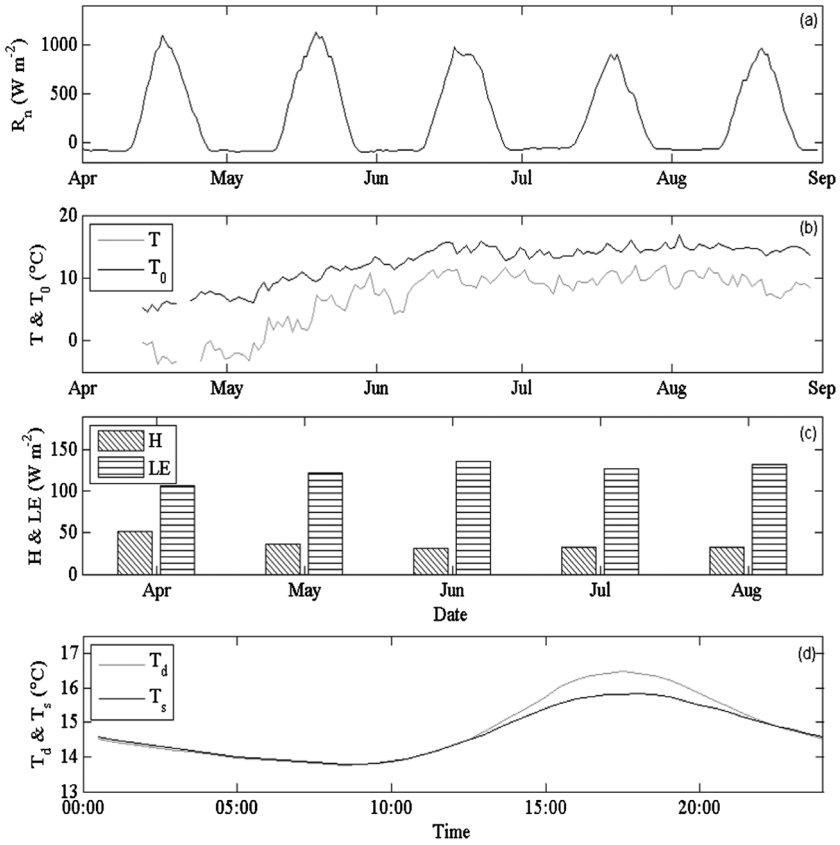

Figure 2. Meteorological observations: (a) monthly-averaged diurnal variation of R_n; (b) daily-averaged T and T_0; (c) monthly-averaged H and LE; and (d) diurnal variation of temperature in a deep layer (T_d) and a shallow layer (T_s) over August.

4. Results and Discussion

4.1. Observing Water and Surface Layer Conditions

Because of the low air density and small optical depth of the atmosphere on the TP, very high net radiation (R_n) is observed at the high-altitude small Nam Co Lake (Figure 2a). Due to strong solar heating, daily mean T_0 increased quickly from 4.5°C on 14 April to approximately 15°C on 13 June, while daily mean T rose from −3.8°C to approximately 11°C over the same period (Figure 2b). We note that daily mean T_0 is higher than daily mean T for the whole observational period, and the average water-atmosphere temperature gradient (ΔT) is approximately 5.4 K. ΔT of small Nam Co Lake is much higher than ΔT of large Lake Ngoring during period of June to August. The temporal variation of ΔT corresponds to a higher H in the beginning of the observational period relative to later in the season (Figure 2c). The LE is much higher than H, and the available energy is primarily consumed by LE. In addition to the large ΔT, there is also very strong wind with an average U_z of 4.8 m s^{-1} and an instantaneous value of over 10 m s^{-1}. Moreover, the large average values for ΔT and U_z from the observational data suggest prevailing unstable and neutral atmospheric conditions in the boundary layer [*Croley*, 1989]. Such atmospheric conditions are also observed and confirmed at a larger high-altitude lake (Lake Ngoring) in *Li et al.* [2015]; they may be related to the higher solar radiation on high-altitude lakes of the TP [*Verburg and Antenucci*, 2010]. In addition, the thermal stratification of lake water (Figure 2d) shows a high temperature in the surface layer (T_s, average value of 9 cm and 15 cm) and a low temperature in the deep layer (T_d, 65 cm), which is attributed to the reduced mixing in the shallow small lake. Generally, assume there is a larger evaporation than precipitation in the small Nam Co Lake, the salinity in the small Nam Co Lake should increase. Although this process leads to extremely large water temperature gradients (solar pond), the observation in the lake do not support the onset of a solar pond-like situation, which may be due to lower salinity subsurface inflow from the large Nam Co Lake.

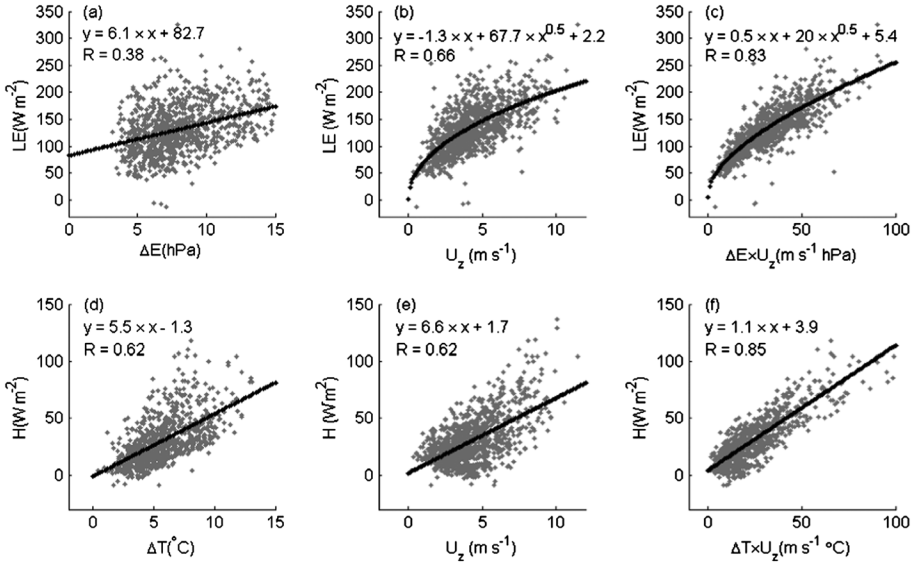

Figure 3. Scatterplots between half-hourly (a) LE and ΔE; (b) LE and U_z; (c) LE and $\Delta E \times U_z$; (d) H and ΔT; (e) H and U_z; and (f) H and $\Delta T \times U_z$. The fitting lines are plotted as dot line with fitting equations and correlation coefficients (R) marked.

The large observed value for U_z and ΔT indicates strong mechanical dynamic and thermal effects of turbulent generation on the small Nam Co Lake. Many environmental factors, such as the intensity of turbulent mixing, ΔT, and the water-atmosphere vapor pressure gradient (ΔE) can affect the turbulent exchange of heat and water vapor [*Nordbo et al.*, 2011; *Zhang and Liu*, 2014]. It has suggested that H is mostly determined by the product of U_z and ΔT ($U_z\Delta T$) [*Liu et al.*, 2009; *Nordbo et al.*, 2011], while the product of U_z and ΔE ($U_z\Delta E$) can best describe LE [*Blanken et al.*, 2000; *Liu et al.*, 2009; *Nordbo et al.*, 2011]. As shown in Figure 3, $U_z\Delta T$ and $U_z\Delta E$ are most highly correlated ($U_z\Delta T$, $R = 0.85$; $U_z\Delta E$, $R = 0.83$) of all the factors. These high-correlation coefficients imply that both the B model and the M model are suitable for modeling water and heat flux with the differences between C_H & C_E and Γ. It is remarkable that U_z shows a much higher-correlation coefficient ($R = 0.66$) than ΔE ($R = 0.38$) for LE and has the same value ($R = 0.62$) as the correlation between ΔT ($R = 0.62$) and H. Respectively, 14.4% and 38.4% of the variability in LE and H can be explained by ΔE and ΔT, while U_z alone explains 43.6% and 38.4% of the variability. The correlation between H, LE, and U_z on a half-hourly time scale is similar to the results for three small lakes in Canada found by *Granger and Hedstrom* [2011]. However, our results differ from those of other studies, such as the poor correlations for the Great Slave Lake in northwest Canada [*Blanken et al.*, 2000], a small boreal lake in southern Finland [*Nordbo et al.*, 2011], and the large Ross Barnett Reservoir in the U.S. [*Zhang and Liu*, 2014]. In a brief summary, wind speed plays an important role in water and heat transport on the high-altitude small Nam Co Lake.

To evaluate the combined effect of temperature and humidity on the air density gradient, we have calculated the gradient in virtual temperature, which was on average 6.5 K over the observation period. The large virtual temperature gradient indicates a large air density gradient, which leads to FCCs. The square root fitting, rather than linear fitting, in Figures 3b and 3c indicates that indeed FCCs had a significant impact on heat and vapor fluxes at the water-air interface. Linear fitting (Figures 3e–3f) was still adequate for sensible heat flux, possibly due to its small magnitude, especially in the low wind speed range, where H is comparable or smaller than instrumental noise. Further evidence is provided later on (see Figure 11).

4.2. Comparison Between Models and Sensitivity Analysis

We compared the simulation results from the B model and the M model. The comparison shows very consistent results, with correlation coefficients of 0.99 for H, LE, and u_* (Figures 4a–4c). However, the H and LE simulated by the B model are approximately 10% and 9% higher, respectively, than those from the M model (Figures 4a and 4b). The similarity between the simulated u_*, H, and LE indicates that the B model (based on flux-profile similarity theory) and the M model (based on experiments and atmospheric stratification theory) are consistent and give similar values when simulating heat flux over the lake water surface.

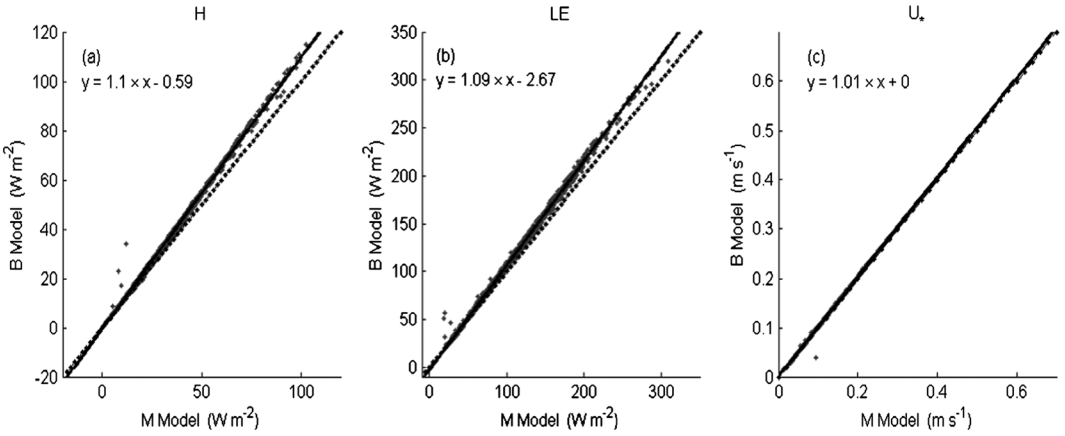

Figure 4. Scatterplots of (a) H, (b) LE, and (c) u_* between the B model and the M model; the 1:1 and linear-fitting lines are shown by the dashed and solid lines, respectively, with fitting equations marked.

Roughness lengths are important parameters in turbulent flux modeling. Uncertainty in the roughness length can result in an overestimation or underestimation of the simulated fluxes. We performed a numerical experiment to analyze the sensitivity of turbulent flux simulations to z_{0m} and z_{0h} in the B model. One hundred groups of z_{0m} and z_{0h} (10 increased $z_{0m} \times 10$ increased z_{0h}) were used to calculate the experimental H, LE, and u_*, with the original z_{0m} and z_{0h} used as reference values. Compared with the reference, the experimental H, LE, and u_* all increased as a result of the larger z_{0m} and z_{0h} (Figures 5c–5e). As z_{0m} will cause a nonlinear change in z_{0h} based on equation (6), the increased ratio of z_{0h} is expressed as a natural logarithm in Figure 5. For example, if both z_{0m} and z_{0h} are multiplied by 6, the experimental z_{0m}, $\ln(z_{0h})$, H, LE, and u_* will increase, respectively, by factors of 9, 3.38, 1.56, 1.59, and 1.28 compared to the original settings. In contrast, a decrease in z_{0m} and z_{0h}, relative to the reference, will also lead to a decrease in H, LE, and u_* in the B model simulations (figure is not shown).

A similar experiment was performed for T_0 and T with variations of ±1 K. Variations in T_0 and T may change the sign of ΔT and thus influence the sign of the simulated H and LE. The simulation results with observed $\Delta T > 2$ K were used for the analysis. The results show that increased (decreased) ΔT can increase (decrease) H and LE, as in Figure 6. For example, the experimental H and LE, relative to the original simulations, increased, respectively, by 13% and 9% when T_0 increased by 0.4 K and T decreased by 0.4 K. Moreover, variations of ±1 K in T_0 and T can result in a variation of ± 33% of H and ± 21% of LE.

4.3. Bias in Roughness Lengths and Fluxes

The above sensitivity analysis showed that z_{0m} and z_{0h}&z_{oq} are important for accurate modeling of water and heat fluxes. The roughness lengths estimated in the model by using "sea parameters" ($\alpha = 0.013$, $R_r = 0.11$) of z_{0m} were compared to observed values (Figure 7). The observed z_{0m} shows a peak-frequency value of 3.35×10^{-4} m (Figure 6a), while the highest-frequency values of the observed z_{0h} and z_{oq} are also at the peak value of 3.35×10^{-4} m (Figure 7b). However, the z_{0m} and z_{0h} derived using sea parameters in the B model peak at 4.1×10^{-5} m and 9.1×10^{-5} m, respectively. The observed z_{0m} is approximately 8 times larger than the value simulated using sea parameters, and the observed z_{0h} and z_{oq} are almost 4 times higher than those derived using sea parameters in the B model. Additionally, even though the peak values of the observed z_{0h} and z_{0q} are the same (Figure 7b), z_{0q} is larger than the corresponding z_{0h} in most of the observations (Figure 7c). Thus, the models' assumption that z_{0h} and z_{0q} are the same is inappropriate.

The fluxes simulated using sea parameters in the B model and the M model were also validated with EC observations. We found that the B model and the M model underestimate H, LE, and u_* (Figure 8). The smaller roughness lengths can lead to lower transfer coefficients and thus reduce the heat flux transport. Statistically, the bias in z_{0m} and z_{0h} means that underestimating z_{0m} and z_{0h} can in turn lead to a 23% underestimation of the simulated H and LE based on sensitivity analysis of the B model. The underestimated roughness lengths in the sea parameters simulations can explain the underestimation of the simulated H and LE. To resolve the

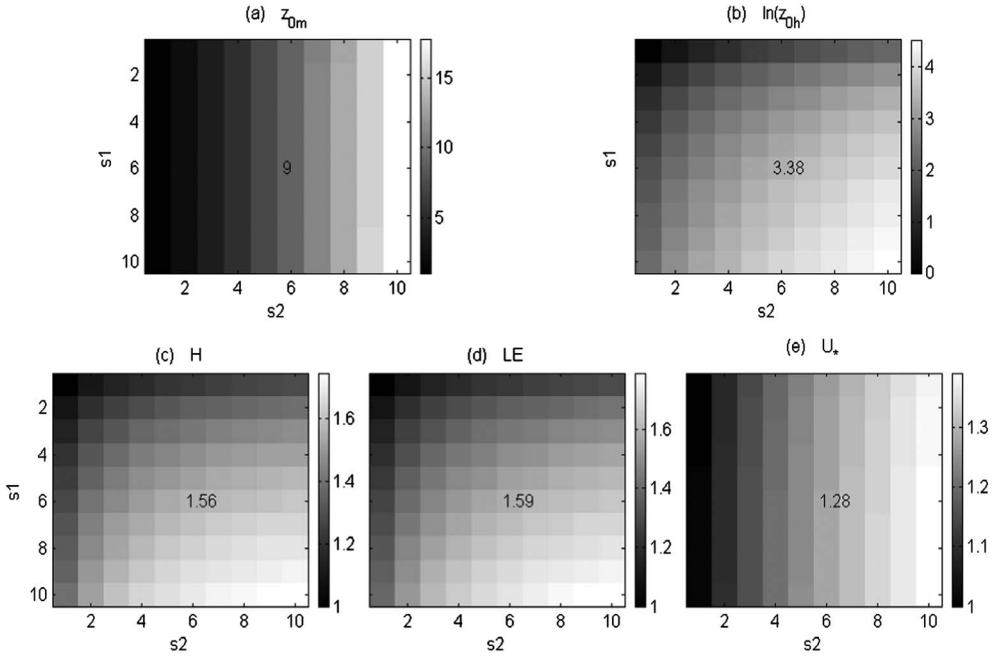

Figure 5. The increased ratios of experimental (a) z_{0m}, (b) $\ln(z_{0h})$, (c) H, (d) LE, and (e) u_* using increased z_{0m} and increased z_{0h} with original simulations as reference; s1 and s2 indicate the multipliers (1 to 10) of z_{0m} and z_{0h}. The increased ratios in Figures 5a–5f represent the slope values of linear-fitting line (passing through the origin) between experimental z_{0m}, z_{0h}, H, LE, u_*, and those from reference simulations; the number in each figure is an example for s1 = s2 = 6.

problem of underestimating z_{0m}, we use the EC observations to optimize z_{0m} by calibrating the Charnock number (α) for rough flow and roughness Reynolds number for smooth flow (R_r) for the small Nam Co Lake.

4.4. Optimization of Roughness Length for Momentum

Respectively, α and R_r are often used to represent the variation in z_{0m} for rough seawater flow and smooth seawater flow [*Charnock*, 1955; *Fairall et al.*, 1996b; *Smith*, 1988]. The methods used to determine α can be divided into three categories [*Gao et al.*, 2006]: (1) constant value or simple wind speed dependence, (2) wave age dependence, and (3) wave steepness dependence. Assuming that the wave field (including wave age and wave steepness) cannot fully develop in the small Nam Co Lake and thus will have limited influence on z_{0m}, we assume that α is constant in the small Nam Co Lake.

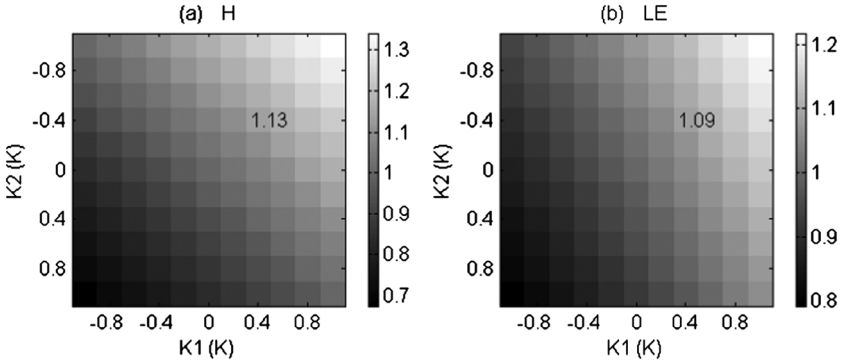

Figure 6. The ratios of change in (a) H and (b) LE using different T_0 and T. K1 and K2 indicate the values of change in T_0 and T (±1 K). The ratios of change in Figures 6a and 6b represent the slope values of linear-fitting line (passing through the origin) between experimental H, LE, and those from reference simulations; the numbers in each figure is an example for K1 = 0.4 K and K2 = −0.4 K.

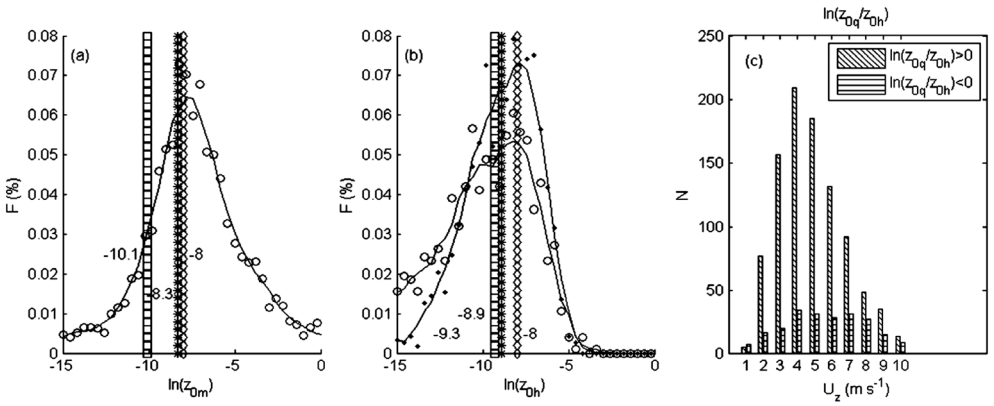

Figure 7. Statistical distribution for (a) $ln(z_{0m})$ and (b) $\ln(z_{0h})$ and $\ln(z_{0q})$; dots are $\ln(z_{0q})$, circles are $\ln(z_{0h})$; (c) $\ln(z_{0q}/z_{0h})$ at each bin of wind speed. The vertical line of squares indicates the peak value of sea parameters simulation in B model ($ln(z_{0m}) = -10.1$, $\ln(z_{0h}) = -9.3$); the vertical line of stars indicate the improved parameter simulation in B model ($ln(z_{0m}) = -8.3$, $\ln(z_{0h}) = -8.9$); the vertical line of diamonds indicate the peak values of observations ($ln(z_{0m}) = \ln(z_{0h}) = \ln(z_{0q}) = -8$); "F" and "N" represent frequency and numbers, respectively.

For rough flow, α is estimated to be 0.011 in open sea conditions and 0.03 in coastal areas [*Sempreviva et al.*, 1990; *Smith*, 1988; *Huang*, 2012]. As most of these studies focused on the sea-atmosphere interaction, we performed a numerical simulation with the B model in which we used observations to optimize the most appropriate α for the small Nam Co Lake. We set α to change from 0.001 to 0.1 with a bin size of 0.001. We compared the simulation results with the EC observations, and the normalized RMSE values for each binned α are shown in Figure 9a: the smallest RMSE values for *H* and LE are achieved when α is 0.012 and 0.036, respectively, with the smallest RMSE value for u_* at 0.031. As z_{0m} is closely related to u_* (the determined momentum flux), we suggest that the optimal value of α for water and heat flux simulation on the small

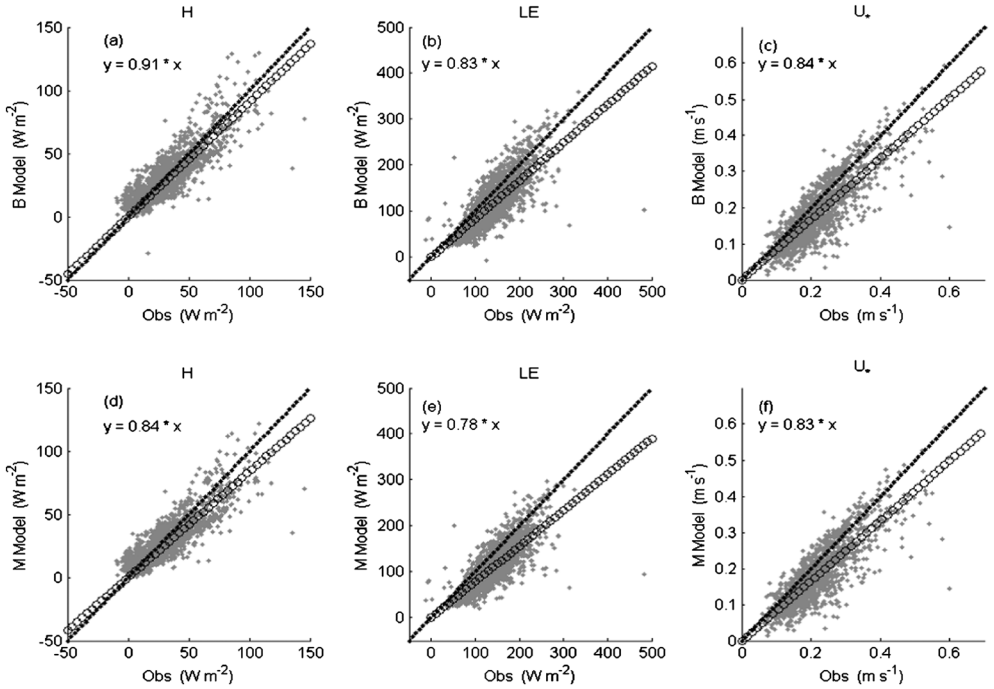

Figure 8. Scatterplots of *H*, LE, and u_* between simulation using sea parameters (the (a–c) B model and the (d–f) M model) and observations (Obs). The 1:1 and linear-fitting lines are shown by the dot and circle lines, respectively, with fitting equations marked.

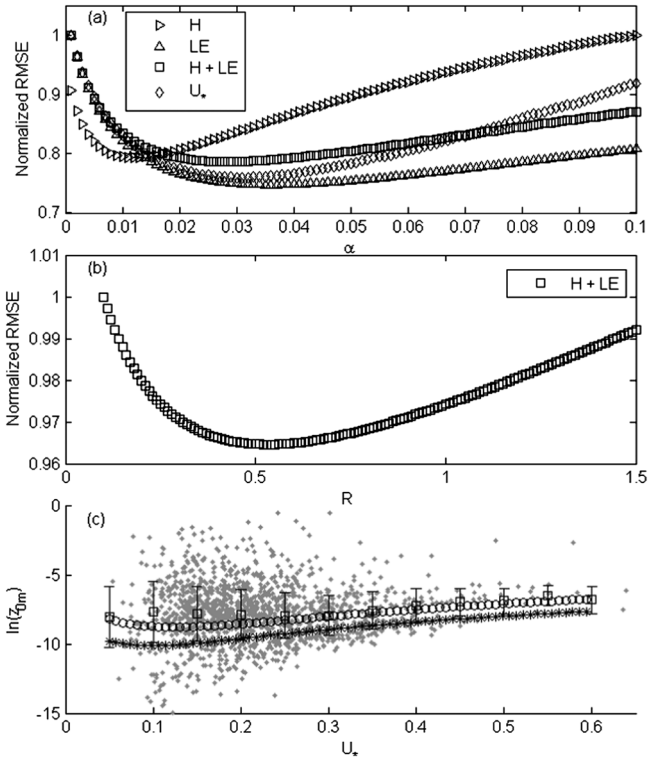

Figure 9. Optimization of z_{0m}: (a) the normalized RMSE for α, normalized values: H, 14.3 W m^{-2}; LE, 47.5 W m^{-2}; H + LE, 60.5 W m^{-2}; u_*, 0.0736; (b) the normalized RMSE for R_r, normalized value: H + LE, 47.74 W m^{-2}; (c) the relationships between ln(z_{0m}) and u_*. The dots are observations; the squares are the mean of observations for each binned u_* (from 0.05 to 0.6 with a bin size of 0.05, error bars are marked); the star and circle lines are fitting lines of ln(z_{0m}) using the sea parameters and the improved parameters, respectively.

Nam Co Lake is 0.031, which is in the range of 0.013–0.035 suggested by *Fairall et al.* [2006]. For smooth flow, a "constant" roughness Reynolds number of $R_r = 0.11$ is used for sea-atmosphere simulations [*Smith*, 1988]. However, for the high-altitude small Nam Co Lake, which has a distinct lake environment and atmospheric conditions, we performed a similar numerical simulation with the B model (with R_r changing from 0.1 to 1.5 with a bin size of 0.001 and $\alpha = 0.031$) to determine its proper value. The simulated results show that the smallest RMSE value for $H + \mathrm{LE}$ is achieved when $R_r = 0.54$ (Figure 9b).

After parameter optimization, the "improved parameters" ($\alpha = 0.031$ and $R_r = 0.54$) z_{0m} result in a much better fit with the observations than the results obtained using the original sea parameters z_{0m} (Figure 8c). Particularly, compared with the results using the original sea parameters z_{0m}, the results obtained using the improved parameters show that z_{0m} increases with a larger α in rough flow (large u_* in Figure 9c) and with a larger R_r in smooth flow (small u_* in Figure 9c). The increase in α is likely related to the larger roughness length for momentum of the shallow water basin where water surface is much rougher due to short wavelength or short wave period [*Gao et al.*, 2009; *Hull*, 1979]. Apparently, the effect of short wavelength is dominant over the effect of smaller wave height, while the increase in R_r may be attributed to the geometry of capillary waves and surface tension [*Bourassa et al.*, 1999; *Wu*, 1994]. In addition, the z_{0m} (2.49×10^{-4} m) simulated using the improved parameters is much closer to the peak frequency of observations (Figure 7a), and the simulated z_{0h} and z_{oq} (1.36×10^{-4} m) also increased with the increased z_{0m} (Figure 7b). Finally, the error metrics of H, LE, and u_* with different parameter combinations are shown in Table 1: the RMSE on LE improves from 37.99 W m^{-2} to 33.49 W m^{-2} and the RMSE of u_* also decreases from 0.059 to 0.052; however, the RMSE on H increases slightly.

Comparing the model simulations with the EC measurements shows that the linear slopes for the B model are 1.04 and 0.96 for H and LE, respectively, while those for the M model are 0.93 and 0.87 (Figure 10). Relative to the M model, the better performance of the B model can be attributed to the optimization of z_{0m}. Moreover, the slope values using the improved parameters (Figure 10) versus the sea parameters (Figure 8) show that H, LE, and u_* are all significantly improved after optimization of z_{0m}. Moreover, the residual underestimation of the M model can be further explained by the model parameters that were kept constant in the fitting**.** These results indicate that model simulation using the sea parameters of z_{0m} greatly underestimates H, LE, and u_*, while a proper parameterization of z_{0m} is vital for accurate heat and water exchange modeling on the high-altitude shallow small lakes.

Statistical evaluations of model performance using improved parameters for z_{0m} are shown in Table 2, where various data quality indicators (1–5) are considered. In general, the R, MAE, and RMSE improve when good quality data are used. The correlation coefficients (R) for H (with quality indicators less than 4) for the B model

Table 1. RMSE of H, LE, and u_* With Different Parameters in z_{0m}

Parameters	RMSE (H, W m^{-2})	RMSE (LE, W m^{-2})	RMSE (u_*)
$\alpha = 0.013$, $R_r = 0.11$	11.36	37.99	0.059
$\alpha = 0.031$, $R_r = 0.11$	11.87	35.72	0.056
$\alpha = 0.031$, $R_r = 0.54$	12.31	33.49	0.052

and the M model are 0.85 and 0.86, respectively. Both values represent an improvement on the results of the variational method (0.72) from *Cao et al.* [2006]. The best values of R, MAE, and RMSE for LE are 0.84, 24.2 W m^{-2} and 31 W m^{-2} for the B model, and 0.85, 26.5 W m^{-2}, and 32.7 W m^{-2} for the M model. The determination coefficient (R^2) and MAE for LE in both models are better than those (0.64 and 30.3 W m^{-2}) from *Biermann et al.* [2013]. As for H, the MAE and RMSE values do not show large variations for either model and the differences with the results of *Biermann et al.* [2013] may be caused by observational uncertainty.

4.5. Limitations of the Models

The relationships between u_*, C_H, and Z_m/L in the B model simulations, observations, and the "observations with FCCs removed" are shown in Figure 11. It is well known that u_* has a high positive correlation with wind speed [*Gao et al.*, 2006]. As indicated in Figures 11a2 and 11a3, when the wind speed is low, because of large temperature gradients, the atmosphere is always in an unstable condition. When wind speed increases, the atmosphere can shift from an extremely unstable condition (for example, FCCs) to a nearly neutral state. This can also be simulated by the B model as shown in Figure 11a1. Figure 11b3 shows a nearly constant mean C_H of approximately 0.00195 for observations with FCCs removed. Simulations with the B model confirm this constant C_H value for $u_* > 0.2$. For $u_* < 0.2$, C_H increases because of FCCs. The increase of C_H in free convection is also shown in Figure 11b2. As for C_E, its value is higher than C_H when $u_* < 0.3$ and it also corresponds to a larger z_{0q} than z_{0h} (Figure 6c). An unstable surface layer will enhance the heat flux transport compared to stable conditions. The average decreasing rate from unstable to near neutral conditions is 0.00051 in the B model simulation (Figure 11c1) and 0.00031 for the observations with FCCs removed (Figure 11c3); a much faster decreasing rate of 0.00073 is associated with the EC observations (Figure 11c2). Therefore, FCCs can

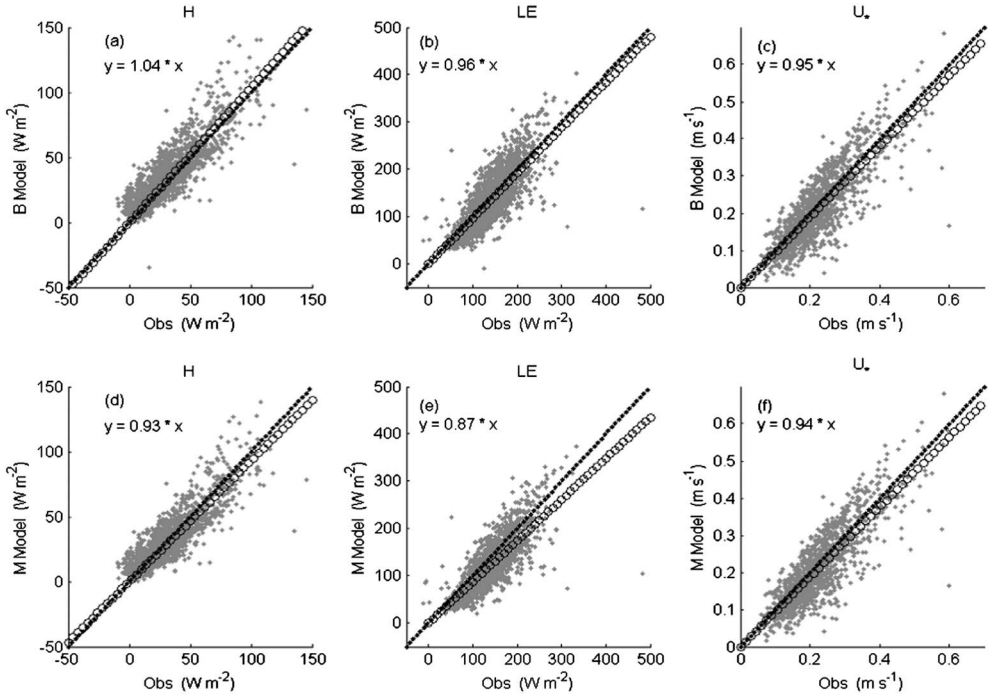

Figure 10. Scatterplots of H, LE, and u_* between simulation using improved parameters (the (a–c) B model and the (d–f) M model) and observations (Obs); the 1:1 and linear-fitting lines are shown by the dot and circle lines, respectively, with fitting equations marked.

Table 2. The *R*, MAE, and RMSE Between the Simulations and the Observations With Different Data Quality Considered

		u_*			LE (W m^{-2})			H (W m^{-2})		
		R	MAE	RMSE	*R*	MAE	RMSE	*R*	MAE	RMSE
1 (high)	B model	0.90	0.032	0.041	0.84	24.2	31.0	0.90	9.2	12.1
	M model	0.90	0.032	0.041	0.85	26.5	32.7	0.90	9.3	11.6
1–3	B model	0.84	0.039	0.052	0.82	25.1	33.5	0.85	8.9	12.3
	M model	0.84	0.039	0.053	0.83	27.7	35.5	0.86	8.3	11.1
1–5 (low)	B model	0.77	0.046	0.065	0.79	26.6	36.8	0.84	9.2	12.6
	M model	0.77	0.046	0.065	0.80	29.3	39.3	0.85	8.5	11.4

significantly enhance the water and heat transfer in the vicinity of the water surface, and the B model can only partially correct these effects through the atmospheric stability correction.

Because of the rapid increase in air temperature influenced by the surrounding land, a stable atmosphere is expected for small lakes during the daytime. However, the small Nam Co Lake shows positive values of *H* and persistent unstable and neutral atmosphere conditions, similar to the larger Lake Ngoring studied by *Li et al.* [2015]. This atmospheric condition together with the observed high wind speeds and large temperature differences may result from the existence of the large Nam Co Lake for two reasons: (1) Nam Co Lake can enhance the wind speed through land-lake breeze circulation; (2) its presence can also reduce air temperatures in the Nam Co Lake basin, as suggested by mesoscale model simulation [*Lv et al.*, 2008]. To summarize briefly, because Nam Co Lake's air inflow causes lower air temperature and higher wind speed, *H* may be enhanced on the small Nam Co Lake, compared with other small lakes on the TP; and the models' performance under stable conditions needs further validation.

The roughness lengths for heat and water are assumed to be the same in the National Centers for Environmental Prediction medium range forecast model and the algorithm in Goddard Earth Observing data assimilation system [*Verburg and Antenucci*, 2010; *Zeng et al.*, 1998]. However, *Fairall et al.* [1996b] gave different values of roughness lengths for temperature and humidity in tropical oceans, and the scalar roughness

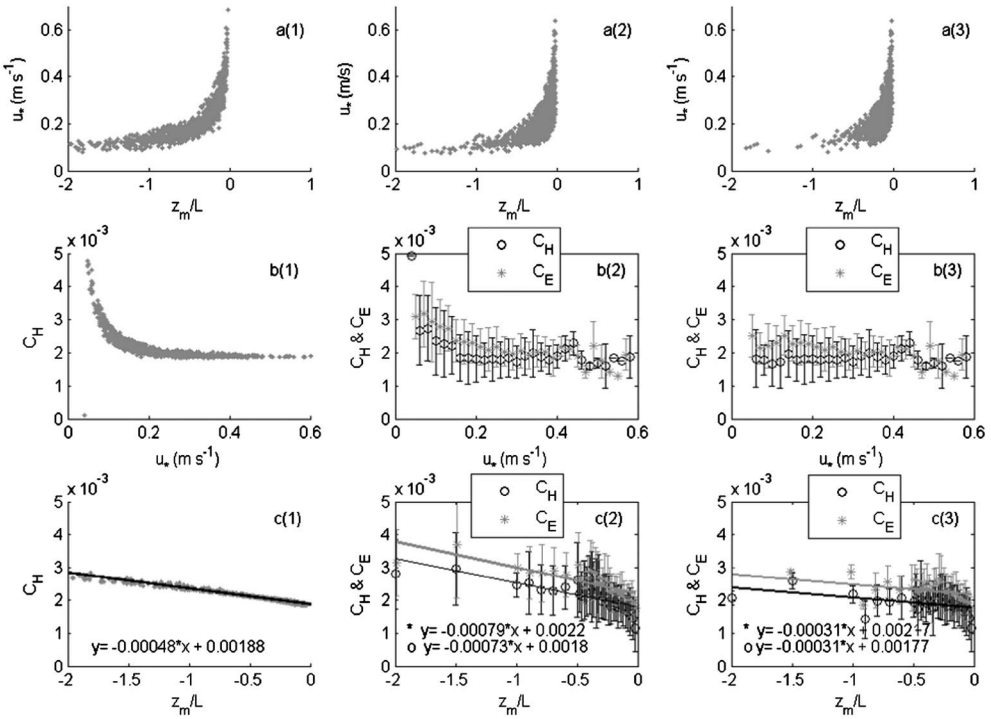

Figure 11. The relationships between C_H/C_E, u_*, and Z_m/L. (a1, b1, and c1) The B model simulation. (a2, b2, and c2) The observations. (a3, b3, and c3) The FCCs removed observations. The vertical bars in Figures 11b2, 11b3 11c2, and 11c3 indicate the standard deviations. Linear-fitting lines are shown in Figures 11c1, 11c2, and 11c3).

length ratio (z_{0h}&z_{0q}) was much larger than unity [*Vickers and Mahrt*, 2010]. Our results suggest a larger z_{0q} than z_{0h} for the small Nam Co Lake, because (1) values of $\ln(z_{0q}/z_{0h})$ larger than unity are more often observed (Figure 7c); (2) H is overestimated while LE is underestimated using the optimized α of 0.031 (Figure 10); and (3) the bulk transfer coefficient is larger for water than for heat (Figure 11). Our results show that the roughness length is higher for water than for heat, which agrees with the results of *Large and Pond* [1982] and the European Centre for Medium-Range Weather Forecasts model [*Zeng et al.*, 1998]. Thus, the assumption that they are the same is inappropriate. Moreover, under FCCs, conventional approaches that use sea-air interactions to determine the roughness length for momentum may also lead to inaccurate results [*Fairall*, 1996]. Adjusting α from 0.013 to 0.031 leads to a limited improvement in model accuracy. However, even without considering factors such as wave age, wave breaking and droplet evaporation effects, lake depth and lake area influence, free convection effects, and cool-skin and warm-layer effects [*Fairall et al.*, 1996a], both models can simulate of heat and water fluxes to an acceptable accuracy.

5. Conclusions

Using data collected in the shallow and small Nam Co Lake over the summer ice-free season of 2012, we reached several conclusions concerning lake-atmosphere heat and water transfer processes on this high-altitude shallow lake. They can be summarized as follows: (1) The observed large water-air temperature gradients and strong winds correspond to the prevailing unstable and near-neutral atmospheric conditions. In these conditions, wind speed plays an important role in lake-atmosphere water and heat flux transport; we emphasize the importance of mechanical dynamic effects. (2) The observed roughness length for momentum is approximately 3.35×10^{-4} m, while the roughness length for water is larger than for heat. Free convection is associated with higher heat bulk transfer coefficients in conditions of low wind speed and an unstable atmosphere; and it gives a square root dependence of latent heat flux on wind speed. Obviously, parameterization schemes for roughness length for heat and water under FCCs should be further improved. (3) The simulations of two models have very high correlation coefficients of 0.99 for H, LE, and u_*, while the values of H and LE from the M model are approximately 10% and 9% lower, respectively, than those from the B model. Given the B model's flexible parameters, relative to the experiment-based constants in the M model, the B model is much easier to improve and apply. (4) Lower estimating the simulated roughness lengths can lead to underestimating the bulk transfer coefficients, which in turn causes an underestimation of the simulated heat flux. The proper values of α and R_r in the roughness length for momentum are estimated to be 0.031 and 0.54, respectively, for this high-altitude shallow lake. The calibrated models can be applied to estimate fluxes under wind directions from land surface for gap filling, which is important for energy balance analysis of the lake. In addition, the optimized parameters in this paper should have a better application prospect than the commonly used sea parameters over the other shallow and small high-altitude lakes on TP. Since the input (lake surface temperature, wind speed, air temperature and humidity) can be obtained from remote sensing products and forcing data sets (such as Moderate Resolution Imaging Spectroradiometer products [*Liang et al.*, 2002] and ITPCAS (Institute of Tibetan Plateau research, Chinese Academy of Sciences) forcing data [*Chen et al.*, 2011]), the calibrated models are well suited to describe lake-atmosphere heat flux in harsh and remote areas of the TP.

Acknowledgments

The data used in this paper can be shared with the scientific public by emailing the corresponding author (wangbinbin@itpcas.ac.cn). This research was funded by China Postdoctoral Science Foundation, the Chinese Academy of Sciences (XDB03030201), the CMA Special Fund for Scientific Research in the Public Interest (GYHY201406001), the National Natural Science Foundation of China (91337212, 41205012, 41275010, 41175008, and 41275028), Chinese Academy of Sciences President's International Fellowship Initiative (2015VEA035), the CAS "Hundred Talent Program" (Weiqiang Ma), and the EU-FP7 "CORE-CLIMAX" projects (313085). Binbin Wang thanks the CSC (China Scholarship Council) for their financial support. We would like to thank the anonymous referees and the Editor for their useful comments and suggestions.

References

Ataktürk, S. S., and K. B. Katsaros (1999), Wind stress and surface waves observed on Lake Washington, *J. Phys. Oceanogr.*, *29*(4), 633–650, doi:10.1175/1520-0485(1999)029<0633:WSASWO>2.0.CO;2.

Beljaars, A. C. M., and A. A. M. Holtslag (1991), Flux parameterization over land surfaces for atmospheric models, *J. Appl. Meteorol.*, *30*, 327–341, doi:10.1175/1520-0450(1991)030<0327:FPOLSF>2.0.CO;2.

Biermann, T., W. Babel, W. Ma, X. Chen, E. Thiem, Y. Ma, and T. Foken (2013), Turbulent flux observations and modelling over a shallow lake and a wet grassland in the Nam Co basin, Tibetan Plateau, *Theor. Appl. Climatol.*, *116*(1), 301–316, doi:10.1007/s00704-013-0953-6.

Blanken, P. D., W. R. Rouse, A. D. Culf, C. Spence, L. D. Boudreau, J. N. Jasper, B. Kochtubajda, W. M. Schertzer, P. Marsh, and D. Verseghy (2000), Eddy covariance measurements of evaporation from Great Slave Lake, Northwest Territories, Canada, *Water Resour. Res.*, *36*(4), 1069–1077, doi:10.1029/1999WR900338.

Blanken, P. D., W. R. Rouse, and W. M. Schertzer (2003), Enhancement of evaporation from a large northern lake by the entrainment of warm, dry air, *J. Hydrometeorol.*, *4*(4), 680–693, doi:10.1175/1525-7541(2003)004<0680:eoefal>2.0.co;2.

Blanken, P. D., C. Spence, N. Hedstrom, and J. D. Lenters (2011), Evaporation from Lake Superior: 1. Physical controls and processes, *J. Great Lakes Res.*, *37*(4), 707–716, doi:10.1016/j.jglr.2011.08.009.

Bourassa, M. A., D. G. Vincent, and W. L. Wood (1999), A flux parameterization including the effects of capillary waves and sea state, *J. Atmos. Sci.*, *56*(9), 1123–1139, doi:10.1175/1520-0469(1999)056<1123:AFPITE>2.0.CO;2.

Brutsaert, W. (1982), *Evaporation Into the Atmosphere: Theory, History, and Applications*, D. Reidel, Dordrecht, Netherlands.

Brutsaert, W. (1999), Aspects of bulk atmospheric boundary layer similarity under free-convective conditions, *Rev. Geophys.*, *37*, 439–451, doi:10.1029/1999RG900013.
Businger, J. A., J. C. Wyngaard, Y. Izumi, and E. F. Bradley (1971), Flux-profile relationship in the atmospheric surface layer, *J. Atmos. Sci.*, *28*, 181–189, doi:10.1175/1520-0469(1971)028<0181:FPRITA>2.0.CO;2.
Cao, Z., J. Ma, and W. R. Rouse (2006), Improving computation of sensible heat flux over a water surface using the variational method, *J. Hydrometeorol.*, *7*(4), 678–686, doi:10.1175/jhm513.1.
Charnock, H. (1955), Wind stress on a water surface, *Q. J. R. Meteorol. Soc.*, *81*(350), 639–640, doi:10.1002/qj.49708135027.
Chen, Y., K. Yang, J. He, J. Qin, J. Shi, J. Du, and Q. He (2011), Improving land surface temperature modeling for dry land of China, *J. Geophys. Res.*, *116*, D20104, doi:10.1029/2011JD015921.
Croley, T. E. (1989), Verifiable evaporation modeling on the Laurentian Great Lakes, *Water Resour. Res.*, *25*(5), 781–792, doi:10.1029/WR025i005p00781.
Daniel, P. E. (1998), A comparison of bulk aerodynamic methods for calculating air-sea flux, Postgraduate thesis, Naval postgraduate school Monterey, Calif.
Deng, B., S. Liu, W. Xiao, W. Wang, J. Jin, and X. Lee (2012), Evaluation of the CLM4 lake model at a large and shallow freshwater lake*, *J. Hydrometeorol.*, *14*(2), 636–649, doi:10.1175/JHM-D-12-067.1.
Donelan, M., F. W. Donelan, S. D. Smith, and R. J. Anderson (1993), On the dependence of sea surface roughness on wave development, *J. Phys. Oceanogr.*, *23*, 2143–2149.
Dyer, A. J. (1967), The turbulent transport of heat and water vapour in an unstable atmosphere, *Q. J. R. Meteorol. Soc.*, *93*(398), 501–508, doi:10.1002/qj.49709339809.
Fairall, C. W. (1996), *Wind, Wave, Stress, and Surface Roughness Relationships From Turbulence Measurements Made on R/P Flip in the SCOPE Experiment a Report for the DoD ASAP Program, Environmental Sensing Program Element (P.ETL.2909)*, U.S. Dep. of Commerce, National Oceanic and Atmospheric Administration, Environmental Research Laboratories, Environmental Technology Laboratory; For Sale by the National Technical Information Service, Boulder, Colo., Springfield, Va.
Fairall, C. W., E. F. Bradley, J. S. Godfrey, G. A. Wick, J. B. Edson, and G. S. Young (1996a), Cool-skin and warm-layer effects on sea surface temperature, *J. Geophys. Res.*, *101*(C1), 1295–1308, doi:10.1029/95JC03190.
Fairall, C. W., E. F. Bradley, D. P. Rogers, J. B. Edson, and G. S. Young (1996b), Bulk parameterization of air-sea fluxes for Tropical Ocean Global Atmosphere Coupled Ocean Atmosphere Response Experiment, *J. Geophys. Res.*, *101*(C2), 3747–3764, doi:10.1029/95JC03205.
Fairall, C. W., L. Bariteau, A. A. Grachev, R. J. Hill, D. E. Wolfe, W. A. Brewer, S. C. Tucker, J. E. Hare, and W. M. Angevine (2006), Turbulent bulk transfer coefficients and ozone deposition velocity in the International Consortium for Atmospheric Research into Transport and Transformation, *J. Geophys. Res.*, *111*, D23S20, doi:10.1029/2006JD007597.
Foken, T. (1979), Vorschlag eines verbesserten Energieaustauschmodells mit Berucksichtigung der molekularen Grenzschicht der Atmosphare, *Z. Meteorol.*, *29*(1), 32–39.
Foken, T. (1984), The paramiterisation of the energy exchange across the air-sea interface, *Dyn. Atmos. Oceans*, *8*, 297–305.
Foken, T. (2008), *Micro-Meteorology*, Springer, Berlin.
Foken, T., and G. Skeib (1983), Profile measurements in the atmospheric near-surface layer and the use of suitable universal functions for the determination of the turbulent energy exchange, *Boundary Layer Meteorol.*, *25*, 55–62, doi:10.1007/BF00122097.
Foken, T., M. Gockede, M. Mauder, L. Mahrt, B. Amiro, and W. Munger (2004), Post-field data quality control, in *Handbook of Micrometeorology*, pp. 181–208, Springer, Netherlands, doi: 10.1007/1-4020-2265-4_9.
Gao, Z., Q. Wang, and S. Wang (2006), An alternative approach to sea surface aerodynamic roughness, *J. Geophys. Res.*, *111*, D22108, doi:10.1029/2006JD007323.
Gao, Z., Q. Wang, and M. Zhou (2009), Wave-dependence of friction velocity, roughness length, and drag coefficient over coastal and open water surfaces by using three databases, *Adv. Atmos. Sci.*, *26*(5), 887–894.
Gerken, T., T. Biermann, W. Babel, M. Herzog, Y. Ma, T. Foken, and H.-F. Graf (2014), A modelling investigation into lake-breeze development and convection triggering in the Nam Co Lake basin, Tibetan Plateau, *Theor. Appl. Climatol.*, *117*(1–2), 149–167, doi:10.1007/s00704-013-0987-9.
Göckede, M., C. Rebmann, and T. Foken (2004), A combination of quality assessment tools for eddy covariance measurements with footprint modelling for the characterisation of complex sites, *Agric. For. Meteorol.*, *127*(3–4), 175–188, doi:10.1016/j.agrformet.2004.07.012.
Granger, R. J., and N. Hedstrom (2011), Modelling hourly rates of evaporation from small lakes, *Hydrol. Earth Syst. Sci.*, *15*(1), 267–277, doi:10.5194/hess-15-267-2011.
Haginoya, S., H. Fujii, T. Kuwagata, J. Xu, Y. Ishigooka, S. Kang, and Y. Zhang (2009), Air-lake interaction features found in heat and water exchanges over Nam Co on the Tibetan Plateau, *Sci. Online Lett. Atmos.*, *5*, 172–175, doi:10.2151/sola.2009-044.
Huang, C. H. (2012), Modification of the Charnock wind stress formula to include the effects of free convection and swell, in *Advanced Methods for Practical Applications in Fluid Mechanics*, edited by S. Jones, InTech. [Available at http://www.intechopen.com/books/advancedmethods-for-practical-applications-in-fluid-mechanics/modification-of-the-charnock-wind-stress-formula-toinclude-the-effects-of-free-convection-and-swell.]
Hull, J. R. (1979), Physics of the solar pond, Retrospective theses and Dissertations. Paper 6608.
Jin, J., N. L. Miller, and N. Schlegel (2010), Sensitivity study of four land surface schemes in the WRF model, *Adv. Meteorol.*, doi:10.1155/2010/167436.
Katsaros, K. B. (1998), Turbulent flux of water vapor in relation to the wave field and atmospheric stratification, in *Physical Processes in Lakes and Oceans*, *Coastal Estuarine Stud.*, vol. 54, edited by J. Imberger, pp. 157–172, AGU, Washington, D. C., doi:10.1029/CE054P0037.
Large, W. G., and S. Pond (1982), Sensible and latent heat flux measurements over the ocean, *J. Phys. Oceanogr.*, *12*(5), 464–482, doi:10.1175/1520-0485(1982)012<0464:salhfm>2.0.co;2.
Lee, X., et al. (2014), The Taihu Eddy Flux Network: An observational program on energy, water, and greenhouse gas fluxes of a large freshwater lake, *Bull. Am. Meteorol. Soc.*, *95*(10), 1583–1594, doi:10.1175/BAMS-D-13-00136.1.
Li, Z., S. Lyu, Y. Ao, L. Wen, L. Zhao, and S. Wang (2015), Long-term energy flux and radiation balance observations over Lake Ngoring, Tibetan Plateau, *Atmos. Res.*, *155*, 13–25, doi:10.1016/j.atmosres.2014.11.019.
Liang, S. L., H. L. Fang, M. Z. Chen, C. J. Shuey, C. Walthall, C. Daughtry, J. Morisette, C. Schaaf, and A. Strahler (2002), Validating MODIS land surface reflectance and albedo products: Methods and preliminary results, *Remote Sens. Environ.*, *83*(1–2), 149–162, doi:10.1016/S0034-4257(02)00092-5.
Liu, H., Y. Zhang, S. Liu, H. Jiang, L. Sheng, and Q. L. Williams (2009), Eddy covariance measurements of surface energy budget and evaporation in a cool season over southern open water in Mississippi, *J. Geophys. Res.*, *114*, D04110, doi:10.1029/2008JD010891.
Liu, H. Z., J. W. Feng, J. H. Sun, L. Wang, and A. L. Xu (2014), Eddy covariance measurements of water vapor and CO_2 fluxes above the Erhai Lake [in Chinese], *Sci. China: Earth Sci.*, *44*, 2527–2539, doi:10.1007/s11430-014-4828-1.

Liu, J., S. Kang, T. Gong, and A. Lu (2010), Growth of a high-elevation large inland lake, associated with climate change and permafrost degradation in Tibet, *Hydrol. Earth Syst. Sci.*, *14*(3), 481–489, doi:10.5194/hess-14-481-2010.
Liu, W. T., K. B. Katsaros, and J. A. Businger (1979), Bulk parameterization of air-sea exchange of heat and water vapor including the molecular constraints at the interface, *J. Atmos. Sci.*, *36*, 1722–1735, doi:10.1175/1520-0469(1979)036<1722:BPOASE>2.0.CO;2.
Lv, Y., Y. Ma, M. Li, and X. Yang (2008), Numerical simulation of typical atmospheric boundary layer characteristics over lake Nam Co region Tibetan Plateau in summer [in Chinese with English abstract], *Plateau Meteorol.*, *25*, 733–740.
Ma, Y., O. Tsukamoto, J. Wang, H. Ishikawa, and I. Tamagawa (2002), Analysis of aerodynamic and thermodynamic parameters over the grassy marshland surface of Tibetan Plateau, *Prog. Nat. Sci.*, *12*, 36–40.
Ma, Y., L. Zhong, Z. Su, H. Ishikawa, M. Menenti, and T. Koike (2006), Determination of regional distributions and seasonal variations of land surface heat fluxes from Landsat-7 Enhanced Thematic Mapper data over the central Tibetan Plateau area, *J. Geophys. Res.*, *111*, D10305, 1–12, doi:10.1029/2005JD006742.
Ma, Y., M. Menenti, R. Feddes, and J. Wang (2008), Analysis of the land surface heterogeneity and its impact on atmospheric variables and the aerodynamic and thermodynamic roughness lengths, *J. Geophys. Res.*, *113*, D08113, doi:10.1029/2007JD009124.
Ma, Y., et al. (2009), Recent advances on the study of atmosphere-land interaction observations on the Tibetan Plateau, *Hydrol. Earth Syst. Sci.*, *13*(7), 1103–1111, doi:10.5194/hess-13-1103-2009.
Mangarella, P. A., A. J. Chambers, R. I. Street, and E. Y. Hsu (1973), Laboratory studies of evaporation and energy transfer through a wavy air-water interface, *J. Phys. Oceanogr.*, *3*, 93–101, doi:10.1175/1520-0485(1973)003<0093:LSOEAE>2.0.CO;2.
Massman, W. J. (1999), A model study of kB for vegetated surfaces using 'localized near-field' Lagrangian theory, *J. Hydrol.*, *223*, 27–43, doi:10.1016/S0022-1694(99)00104-3.
Mauder, M., and T. Foken (2015), Eddy-covariance software TK3, *Zenodo*, doi:10.5281/zenodo.20349.
Menenti, M., and J. C. Ritchie (1994), Estimation of effective aerodynamic roughness of Walnut Gulch watershed with laser altimeter measurements, *Water Resour. Res.*, *30*(5), 1329–1337, doi:10.1029/93WR03055.
Merlivat, L., and M. Coantic (1975), Study of mass transfer at the air-water interface by an isotopic method, *J. Geophys. Res.*, *80*, 3455–3464, doi:10.1029/JC080i024p03455.
Miehe, G., et al. (2011), Plant communities of central Tibetan pastures in the Alpine Steppe/Kobresia pygmaea ecotone, *J. Arid Environ.*, *75*(8), 711–723, doi:10.1016/j.jaridenv.2011.03.001.
Monin, A. S., and A. M. Yaglom (1965), *Statisticeskaja Gidromechanika*, 640 pp., Izd. Nauka, Moskva.
Nordbo, A., S. Launiainen, I. Mammarella, M. Leppäranta, J. Huotari, A. Ojala, and T. Vesala (2011), Long-term energy flux measurements and energy balance over a small boreal lake using eddy covariance technique, *J. Geophys. Res.*, *116*, D02119, doi:10.1029/2010JD014542.
Panin, G. N., and T. Foken (2005), Air-sea interaction including a shallow and coastal zone, *J. Atmos. Ocean Sci.*, *10*(3), 289–305, doi:10.1080/17417530600787227.
Panin, G. N., A. E. Nasonov, T. Foken, and H. Lohse (2006), On the parameterisaton of evaporation and sensible heat exchange for shallow lakes, *Theor. Appl. Climatol.*, *85*(3–4), 123–129, doi:10.1007/s00704-005-0185-5.
Panofsky, H. A., and J. A. Dutton (1984), *Atmospheric Turbulence*, 397 pp., Wiley-Interscience, New York.
Pond, S., D. B. Fissel, and C. A. Paulson (1974), A note on bulk aerodynamic coefficients for sensible heat and moisture fluxes, *Boundary Layer Meteorol.*, *6*, 333–339.
Qiu, J. (2008), The third pole, *Nature*, *454*, 393–396, doi:10.1038/454393a.
Rouse, W. R., C. M. Oswald, J. Binyamin, P. D. Blanken, W. M. Schertzer, and C. Spence (2003), Interannual and seasonal variability of the surface energy balance and temperature of Central Great Slave Lake, *J. Hydrometeorol.*, *4*, 720–730.
Sempreviva, A., S. E. Larsen, N. G. Mortensen, and I. Troen (1990), Response of neutral boundary layers to changes of roughness, *Boundary Layer Meteorol.*, *50*(1–4), 205–225, doi:10.1007/BF00120525.
Smith, S., et al. (1992), Sea surface wind stress and drag coefficients: The hexos results, *Boundary Layer Meteorol.*, *60*(1–2), 109–142, doi:10.1007/bf00122064.
Smith, S. D. (1988), Coefficients for sea surface wind stress, heat flux, and wind profiles as a function of wind speed and temperature, *J. Geophys. Res.*, *93*(C12), 15,467–15,472, doi:10.1029/JC093iC12p15467.
Spence, C., P. D. Blanken, N. Hedstrom, V. Fortin, and H. Wilson (2011), Evaporation from Lake Superior: 2: Spatial distribution and variability, *J. Great Lakes Res.*, *37*(4), 717–724, doi:10.1016/j.jglr.2011.08.013.
Tanaka, K., H. Ishikawa, I. T. Hayashi, and Y. Ma (2001), Surface energy budget at Amdo on Tibetan Plateau using GAME/Tibet IOP'98 data, *J. Meteorol. Soc. Jpn.*, *79*(1B), 505–517.
Tanaka, K., I. Tamagawa, H. Ishikawa, Y. Ma, and Z. Hu (2003), Surface energy budget and closure of the eastern Tibetan Plateau during the GAME/Tibet IOP 1998, *J. Hydrol.*, *283*, 169–283.
Taylor, P., R. I. Sykes, and P. Mason (1989), On the parameterization of drag over small-scale topography in neutrally-stratified boundary-layer flow, *Boundary Layer Meteorol.*, *48*(4), 409–422, doi:10.1007/BF00123062.
Venalainen, A., M. Frech, and M. Heikinheimo (1999), Comparison of latent and sensible heat fluxes over boreal lakes with concurrent fluxes over a forest: Implications for regional averaging, *Agric. Forest. Meteorol.*, *98–99*, 535–546.
Verburg, P., and J. P. Antenucci (2010), Persistent unstable atmospheric boundary layer enhances sensible and latent heat loss in a tropical great lake: Lake Tanganyika, *J. Geophys. Res.*, *115*, D11109, doi:10.1029/2009JD012839.
Vickers, D., and L. Mahrt (2010), Sea-surface roughness lengths in the midlatitude coastal zone, *Q. J. R. Meteorol. Soc.*, doi:10.1002/qj.617.
Vincent, A. C., D. R. Mueller, and W. F. Vincent (2008), Simulated heat storage in a perennially ice-covered high Arctic Lake: Sensitivity to climate change, *J. Geophys. Res.*, *113*, C04036, doi:10.1029/2007JC004360.
Wang, J., L. Zhu, J. Ju, and Y. Wang (2009), Water chemistry of eastern Nam Lake area and in flowing rivers in Tibet, *Sci. Geogr. Sin. (in Chinese)*, *29*(2), 288–293.
Wang, S., and H. Dou (1998), *An Overview of Lakes Over China* [in Chinese], Science Press, Beijing.
Wang, X., P. Gong, Y. Zhao, Y. Xu, X. Cheng, Z. Niu, Z. Luo, H. Huang, F. Sun, and X. Li (2013), Water-level changes in China's large lakes determined from ICESat/GLAS data, *Remote Sens. Environ.*, *132*, 131–144, doi:10.1016/j.rse.2013.01.005.
Webb, E. K., G. I. Pearman, and R. Leuning (1980), Correction of flux measurements for density effects due to heat and water vapour transfer, *Q. J. R. Meteorol. Soc.*, *106*(447), 85–100, doi:10.1002/qj.49710644707.
Wei, D., X. Ri, Y. Wang, Y. Wang, Y. Liu, and T. Yao (2012), Responses of CO_2, CH_4 and N_2O fluxes to livestock exclosure in an alpine steppe on the Tibetan Plateau, China, *Plant Soil*, *359*(1–2), 45–55, doi:10.1007/s11104-011-1105-3.
Whalin, R. W., F. E. Camfield, N. E. Parker, R. A. Jachowski, and J. R. Wegger (1984), *Shore Protection Manual*, vol. 1, 4th., p. 337 ed., U.S. Army Corps of Engineers, Dep. of the Army, Washington, D. C.

Wilczak, J. M., S. P. Oncley, and S. A. Stage (2000), Sonic anemometer tilt correction algorithms, *Boundary Layer Meteorol.*, *99*, 127–150, doi:10.1023/A:1018966204465.

Wu, J. (1994), The sea surface is aerodynamically rough even under light winds, *Boundary Layer Meteorol.*, *69*(1–2), 149–158, doi:10.1007/BF00713300.

Xiao, W., S. Liu, W. Wang, D. Yang, J. Xu, C. Cao, H. Li, and X. Lee (2013), Transfer coefficients of momentum, heat and water vapour in the atmospheric surface layer of a large freshwater lake, *Boundary Layer Meteorol.*, *148*(3), 479–494, doi:10.1007/s10546-013-9827-9.

Yang, K., T. Koike, H. Fujii, K. Tamagawa, and N. Hirose (2002), Improvement of surface flux parametrizations with a turbulence-related length, *Q. J. R. Meteorol. Soc.*, *128*, 2073–2087, doi:10.1256/003590002320603548.

Yang, K., T. Koike, H. Ishikawa, J. Kim, X. Li, H. Liu, S. Liu, Y. Ma, and J. Wang (2008), Turbulent flux transfer over bare-soil surfaces: Characteristics and parameterization, *J. Appl. Meteorol. Climatol.*, *47*(1), 276–290, doi:10.1175/2007JAMC1547.1.

Yang, K., H. Wu, J. Qin, C. Lin, W. Tang, and Y. Chen (2014), Recent climate changes over the Tibetan Plateau and their impacts on energy and water cycle: A review, *Global Planet. Change*, *112*, 79–91, doi:10.1016/j.gloplacha.2013.12.001.

Zeng, X., M. Zhao, and R. E. Dickinson (1998), Intercomparison of bulk aerodynamic algorithms for the computation of sea surface fluxes using TOGA COARE and TAO data, *J. Clim.*, *11*, 2628–2644, doi:10.1175/1520-0442(1998)011<2628:IOBAAF>2.0.CO;2.

Zhang, G., H. Xie, S. Kang, D. Yi, and S. F. Ackley (2011), Monitoring lake level changes on the Tibetan Plateau using ICESat altimetry data (2003–2009), *Remote Sens. Environ.*, *115*(7), 1733–1742, doi:10.1016/j.rse.2011.03.005.

Zhang, G., T. Yao, H. Xie, K. Zhang, and F. Zhu (2014), Lakes' state and abundance across the Tibetan Plateau, *Chin. Sci. Bull.*, *59*(24), 3010–3021, doi:10.1007/s11434-014-0258-x.

Zhang, Q., and H. Liu (2014), Seasonal changes in physical processes controlling evaporation over inland water, *J. Geophys. Res. Atmos.*, *119*, 9779–9792, doi:10.1002/2014JD021797.

Zhou, D., R. Eigenmann, W. Babel, T. Foken, and Y. Ma (2011), The study of near-ground free convection conditions at Nam Co station on the Tibetan Plateau, *Theor. Appl. Climatol.*, *105*(1–2), 217–228, doi:10.1007/s00704-010-0393-5.

Zhou, S., S. Kang, F. Chen, and D. R. Joswiak (2013), Water balance observations reveal significant subsurface water seepage from Lake Nam Co, south-central Tibetan Plateau, *J. Hydrol.*, doi:10.1016/j.jhydrol.2013.03.030.